RSC Advances

PAPER

View Article Online
View Journal | View Issue

Cite this: *RSC Adv.*, 2020, **10**, 31936

Recovery of scandium and neodymium from blast furnace slag using acid baking–water leaching†

Jihye Kim [a] and Gisele Azimi*[ab]

Received 2nd July 2020
Accepted 12th August 2020

DOI: 10.1039/d0ra05797e

rsc.li/rsc-advances

The current study puts the emphasis on developing a pyro-hydrometallurgical process, called acid baking–water leaching, to recover scandium and neodymium from blast furnace slag produced by the ironmaking industry. In this process, the feed is mixed with concentrated sulfuric acid, digested at 200–400 °C, and leached in water at ambient conditions. This process offers several advantages including less acidic waste generation and rapid kinetics. With fundamental investigations into the digestion mechanism, acid to slag mass ratio and baking temperature are determined to have the most significant positive and negative impacts, respectively. At low acid to slag ratio, the silicate bearing phases in the feed do not digest, resulting in low extraction. At 200 °C baking temperature, a hydrated aluminum sulfate ($(Al(H_2O)_6)_2(SO_4)_3(H_2O)_{4.4}$) phase with weak hydrogen bonds is formed that leaches in water rapidly (<10 min); while at 400 °C, $Al_2(SO_4)_3$ with strong ionic bonds is formed that leaches at slower kinetics (>4 h). Fundamental investigations into the water leaching process indicate that the diffusion of water through the firm solid product (ash layer) is the rate determining step. We expect the results of this study would help enable valorization of industrial byproducts, in particular ironmaking slag.

Introduction

Worldwide resource consumption has reached 90 billion metric tons annually and it is expected to double or more by 2050.[1] The extensive growth has raised questions about long term availability of primary resources and sustainability of resource recovery processes. Most primary extraction processes are environmentally unsustainable, as they are energy intensive, consume large volumes of chemical reagents, and produce large volumes of hazardous wastes and environmental pollutions. Hence, the recovery of materials from secondary resources such as industrial byproducts, mine tailings, and waste electrical and electronic equipment has gained interest for reducing the reliance on primary resources and enhancing sustainability.[1,2] Technospheric mining, *i.e.*, recovery from secondary resources can help close materials' life cycle to enable the circular economy.

Among the commodity metals, iron and steel are by far the most widely used materials with annual production near 1.9 billion metric tons.[3] The main byproduct of ironmaking is iron slag, so-called blast furnace (BF) slag, which is generated when iron ore is mixed with flux (limestone and/or dolomite) and coke for fuel and heated under reducing conditions at above 1500 °C, producing molten iron and molten slag. World production of iron slag is estimated at 25–30% of crude (pig) iron production, and in 2019, world iron slag production was estimated to be between 320 and 384 million tons. It is estimated that about 90% of produced BF slag is utilized and about 10% is disposed of in landfills.[4]

Different forms of BF slag are produced depending on the method used to cool the molten slag. These products include air-cooled blast furnace slag (ACBFS), expanded or foamed slag, pelletized slag, and grand granulated blast furnace slag (GGBFS) among which ACBFS and GGBFS are the most common ones.[5,6] Air-cooled iron slag is used primarily as aggregates in concrete, asphaltic paving, fill, and road bases as well as a feed for cement kilns.[7] Almost all GGBFS is used as a partial substitute for Portland cement in concrete mixes or blended cement.[8,9] Pelletized slag is generally used for lightweight aggregates but can be ground into a material similar to GGBFS. Foamed slag is used as a lightweight aggregate for Portland cement concrete, but its production is less common and is being replaced by the pelletizing procedure. Among the four slags, GGBFS has the highest value of up to $120 per ton reported in 2019 in the United States.[4]

Since 10% of produced BF slag (32–38 million tons annually) is landfilled, it is highly desirable to find potential applications for that. Several studies have reported the presence of critical metals, including titanium, niobium, tantalum, and rare earth elements (REEs) in BF slags that can be valorized, bringing additional value to this byproduct.[10,11]

[a]*Laboratory for Strategic Materials, Department of Chemical Engineering and Applied Chemistry, University of Toronto, 200 College Street, Toronto, Ontario, M5S 3E5, Canada. E-mail: g.azimi@utoronto.ca*

[b]*Department of Materials Science and Engineering, University of Toronto, 184 College Street, Toronto, Ontario, M5S 3E4, Canada*

† Electronic supplementary information (ESI) available. See DOI: 10.1039/d0ra05797e

The chemical composition of BF slag depends on the type of ore, flux, and coke purity. The major elements present in BF slag are aluminum, manganese, calcium, iron, magnesium, silicon, and sulfur. There are also small amounts of minor elements such as barium, carbon, and phosphorus as well as environmentally hazardous elements such as arsenic, chromium, and lead. In such cases, slag inertization and hazardous element removal must be conducted prior to slag valorization.[12,13]

The BF slag containing REEs is receiving increasing attention because of the supply chain vulnerability and versatile applications of these elements. Typically, BF slag contains a few dozen mg kg^{-1} of REEs which come from the ore or the coal used.[11,14,15] In the smelting process, iron, phosphorous, and niobium are reduced but REEs are not; thus, they concentrate into the slag. Among REEs, cerium and lanthanum can trap oxygen and sulfur for which they have high affinity. This is beneficial for the process because these two elements deteriorate the properties of steel.[15]

The REEs have unique physicochemical properties; thus, some REEs have become the building block of many critical and emerging green technologies. Neodymium is one of the critical REEs with increasingly high demand (estimated at 700% within the next 25 years) because of its unique magnetic properties. Its alloy with iron and boron is widely used as permanent magnets utilized in wind turbines and electric vehicles. It is also the main component of nickel metal hydride battery utilized in hybrid vehicles. Another critical REE that is receiving growing attention is scandium. Alloying scandium into aluminum products results in stronger, weldable, more corrosion resistant, and heat tolerant aluminum products. Aircraft manufacturers are particularly interested in these alloys because the ability to employ weldable structures results in 15–20% weight reduction in aircraft, which in turn would result in a significant reduction in fuel consumption.[16]

On the basis of the historic data, for some REEs, the supply will not sustain the increasing demand because of the time lags in bringing new production capacity online.[17,18] This stimulated many countries to investigate alternative secondary resources for these elements to tackle their supply challenge.[19] Considering the huge volume of BF slag produced annually and the portion that is stockpiled, it can secure an independent source of REEs for resource-poor countries to satisfy their demand.

Since BF slag is a lean source of REEs, in order to be a competitive source for REEs, it needs to have some of these features: (1) use lower-cost leaching process, (2) have high extraction efficiency, or (3) have its processing costs covered by the value of another primary product. There have been several studies that investigated the recovery of REEs from stocks of landfilled industrial process residues such as phosphogypsum,[20,21] bauxite residue,[16,22] coal fly ash,[23,24] and BF slag.[15] Most previous studies have utilized direct acid leaching processes with HCl, HNO_3, and H_2SO_4 as the leaching agents. To achieve higher extractions, they utilized higher acid concentration, which on the negative side, increases the co-extraction of impurities such as iron, aluminum, and calcium. Moreover, many studies utilized small solid to liquid (S/L) ratios, which has the disadvantage of producing large volumes of very acidic wastewater and residue.[25,26] Furthermore,

Table 1 A summary of previous studies on the recovery of REEs from different sources using acid baking–water leaching

Target element	Reference	Feed	Acid	Baking T (°C)	Acid to feed mass ratio	Baking time (min)	Leachant	Leaching T (°C)	Leachant to solid ratio (mL g^{-1})	Leaching time (min)	Maximum extraction efficiency (%)
Ce, Nd, Sm, Sc	Anawati and Azimi, 2019 (ref. 25)	Bauxite residue	98 wt% H_2SO_4	200–400	1.1–2.4	60–120	Water	25	4–15	120	87, 97, 80, 80
La, Ce, Nd, Y	Soltani *et al.*, 2018 (ref. 31)	Fluorapatite concentrate	95–97 wt% H_2SO_4	190–270	2–3	60–180	Water	25	5–10	60	~85
La, Ce, Pr, Nd, Sm, Eu, Gd, Tb, Dy, Ho, Er, Tm, Yb, Lu, Y	Demol *et al.*, 2018 (ref. 32)	Monazite concentrate	96 wt% H_2SO_4	200–800	1.7	120	0.9 M H_2SO_4	20–25	40	120	99
La, Ce, Pr, Nd, Sm	Meshram *et al.*, 2017 (ref. 33)	Spent NiMH batteries	98 wt% H_2SO_4	100–400	0.46–2.76	30–120	Water or 1 M H_2SO_4	30–95	5–50	5–120	96

some studies have reported high silica dissolution during acid leaching, which can lead to silica gel polymerization resulting in reduced extraction.[27]

To overcome the challenges associated with direct leaching, some studies have investigated multi-stage processes, including microwave pretreatment prior to acid leaching,[16,28] dry digestion,[29] acid roasting–water leaching, and acid baking–water leaching. In the last three techniques, the feed is mixed with concentrated acid (HCl (37 vol%) or H_2SO_4 (95–97 wt%)) and digested at room temperature, above 700 °C, or between 200 and 400 °C, respectively, and the digested sample is leached in water. Dry digestion has the advantage of low operating temperature and fast water leaching kinetics with no silica gel formation, but its acid consumption is the highest among the three.[29] Acid roasting has the advantage of low impurity co-extraction, but it involves high operating temperature, slow water leaching kinetics, and silica gel polymerization in some cases.[30] Acid baking has the advantages of the other two processes including lower operating temperature, but fast water leaching kinetics, with no silica gel formation. In this process, the exhaust gases ($SO_{3(g)}$ and $SO_{2(g)}$) generated during the acid baking step could be condensed and recovered as sulfuric acid, which can be directly used for the acid baking step, making the process more economic.[25] Baking the feed with highly concentrated acid at high temperature allows to achieve high extraction efficiency in relatively short processing time and consequentially to reduce the volume of the final leachate product. Moreover, this process is highly applicable to the iron slag valorization because the remaining heat from the blast furnace (>1500 °C) can be used to heat the mixture of slag and acid during the acid baking step.

A few studies have investigated the acid baking–water leaching process for the recovery of REEs from different resources such as bauxite residue,[25] fluorapatite concentrate,[31] monazite concentrate,[32] and spent nickel metal hydride battery,[33] a summary of which is provided in Table 1. However, to the best of our knowledge, no previous study has investigated the recovery of REEs from BF slag using this process. Moreover, there is a lack of data on the mechanism of this process for REE extraction from this secondary resource.

In this study, an acid baking–water leaching process was developed to recover REEs, mainly scandium and neodymium from BF slag. Through systematic fundamental and experimental investigations, the optimum operating conditions in terms of baking temperature, acid to slag mass ratio, baking time, water to acid-baked slag ratio, agitation rate, and water to slag mass ratio was determined. Using statistical analyses, the effect of each operating parameter was quantified, and empirical models were built to predict the optimum operating conditions that result in maximum scandium and neodymium extraction. Moreover, fundamental investigations were carried out to elucidate the acid digestion and water leaching process mechanisms, which can help develop the process with high efficiency.

Experimental

Materials

The BF slag was obtained from an undisclosed source (ESI Fig. S1†). Porcelain crucibles were supplied by Chemglass Life Sciences LLC (Vineland, NJ, USA). All chemicals were of analytical grade purity and used without further purification. Sulfuric acid (95.0–98.0 wt% assay), hydrochloric acid (36.5–38.0 vol% assay), and nitric acid (68.0–70.0 wt% assay) were purchased from VWR (Radnor, PA, USA). Deionized water was produced by Milli-Q Integral water purification system (0.055 μS cm^{-1}, MilliporeSigma, Merck KGaA, Darmstadt, Germany). The standard stock solution of REEs (100 mg L^{-1}) and that of base metals (Ca, Al, Mg, Fe, Ti, K, Mn, and Na) (1000 mg L^{-1}) were purchased from Inorganic Ventures, Inc. (Christiansburg, VA, USA).

Experimental procedure

The block flow diagram of the acid baking–water leaching process is shown in ESI Fig. S2.† The BF slag sample was crushed and ground utilizing a ball mill (Galigher Co., Slat Lake, UT, USA) to obtain a uniform particle size of −200 mesh (−74 μm) for the sample homogeneity (ESI Fig. S3†). The ground slag was dried in an oven for more than 24 h, manually mixed with concentrated sulfuric acid (95.0–98.0% assay) using a glass rod in a porcelain crucible, and baked in a box furnace (Ney Vulcan furnace, Gesswein Canada, Toronto, ON, Canada) at 200–400 °C. The acid-baked sample was then leached in the water at room temperature (25 °C) for 6 h using a magnetic stirrer (Corning PC-420D, Corning, NY, USA). The leachate solution was sampled at specified time intervals and filtered using a 0.45 μm nylon syringe filter (Fisher Scientific, Waltham, MA, USA). The filtered sample was diluted with 5 wt% HNO_3 using Hamilton Microlab 600 diluter/dispenser system (Hamilton Company, Reno, NV, USA). Kinetic tests were conducted using a temperature-controlled water bath (Fisherbrand Isotemp 4100 H21P, Fisher Scientific) following the same sampling procedure.

Factorial design of experiments

A systematic investigation was performed with an emphasis on the effect of six operating parameters, *i.e.*, baking temperature (X_1), acid to slag mass ratio (X_2), baking time (X_3), water to acid-baked slag ratio (X_4), agitation rate (X_5), and water to slag mass ratio (before baking) (X_6) on the extraction of scandium and neodymium. These parameters were coded to three levels (−1, 0, and +1) to directly compare the effect of the parameters. The upper and lower bounds of the variables were determined on the basis of preliminary experiments. A detailed description of the operating parameters is presented in ESI Table S1.†

Empirical model building

To build an empirical extraction model, a $2_{IV}{}^{6-2}$ experimental matrix at fixed leaching time (6 h) was designed utilizing a fractional factorial design of experiment methodology (ESI Table S2†). Next, the model of the format shown in eqn (1) was fitted to the extraction efficiency data by multiple Linear Least Squares Regression (mLLSR, eqn (2)). The simplified models including only the significant parameters (significance level: $\alpha = 0.05$) were assessed by analysis of variance (ANOVA) to adequately estimate the run variance. Furthermore, kinetic tests were carried out at the lower and upper boundary of baking

temperature while other parameters were kept at the zero (mid) level, to study the effect of baking temperature on the kinetics of the water leaching process.

$$\hat{y}_i = \hat{\beta}_0 + \hat{\beta}_1 X_1 + \hat{\beta}_2 X_2 + \hat{\beta}_3 X_3 + \hat{\beta}_4 X_4 + \hat{\beta}_5 X_5 + \hat{\beta}_6 X_6 \quad (1)$$

where $\hat{\beta}$ is the vector containing each of the model parameters, $\hat{\beta}_0$ corresponds to the baseline bias for the analyte, $\hat{\beta}_1$ corresponds to the baking temperature, $\hat{\beta}_2$ corresponds to the acid to slag mass ratio, $\hat{\beta}_3$ corresponds to the baking time, $\hat{\beta}_4$ corresponds to the water to acid-baked slag ratio, $\hat{\beta}_5$ corresponds to agitation rate, and $\hat{\beta}_6$ corresponds to the water to slag mass ratio (before baking).

$$\hat{\beta} = (X^T X)^{-1}(X^T Y_i) \quad (2)$$

where X is the experimental design matrix (Table S2†), and Y_i is the response matrix including the actual extraction efficiencies for analyte i. A more detailed description of the empirical model building methodology is presented in the ESI.†

Compositional, mineralogical, morphological, thermogravimetric, and particle size analysis

To determine the elemental composition of the feed, BF slag (dry) samples were digested in 20 mL of *aqua regia* at 220 °C by MARS 6 Xpress microwave digestion system (ramp-up time of 40 min, holding time of 30 min, CEM Corporation, Matthews, NC, USA) and characterized with inductively coupled plasma mass spectrometry for REEs (ICP-MS, Thermo Scientific iCAP Q, Waltham, MA, USA) and inductively coupled plasma optical emission spectroscopy (ICP-OES, PerkinElmer Optima 8000, Waltham, MA, USA) for other elements. The silicon content was measured using X-ray fluorescence spectrometer (XRF, Bruker S2 Ranger, Billerica, MA, USA). The mineralogical analysis of the sample was performed with X-ray diffraction (XRD) (Rigaku MiniFlex 600 diffractometer). Morphological characterization of the samples was obtained with scanning electron microscopy energy dispersive spectroscopy (SEM-EDS, Hitachi SU 3500, Krefeld, NRW, Germany). The thermogravimetric analysis was performed using thermogravimetry-differential scanning calorimetry (TG-DSC, Netzsch STA 449 F3 Jupiter, Wunsiedel, Bavaria, Germany). Particle size analysis was carried out by a laser particle size analyzer (Horiba Partica LA-950, Minami-ku, Kyoto, Japan).

Results and discussion

Characterization of BF slag

The chemical composition of the BF slag was analyzed to provide a basis for calculating extraction efficiencies. The main REEs present are scandium (Sc), yttrium (Y), lanthanum (La), cerium (Ce), praseodymium (Pr), neodymium (Nd), samarium (Sm), gadolinium (Gd), and dysprosium (Dy), with a total REE concentration of 356 mg kg^{-1}. The bulk elements are calcium (Ca, 21.7 wt%), silicon (Si, 13.7%), aluminum (Al, 6.8 wt%), magnesium (Mg, 6.5 wt%), and iron (Fe, 1.0 wt%) with small quantities of titanium (Ti, 0.37 wt%), potassium (K, 0.35 wt%), manganese (Mn, 0.27 wt%), and sodium (Na, 0.21 wt%) (as

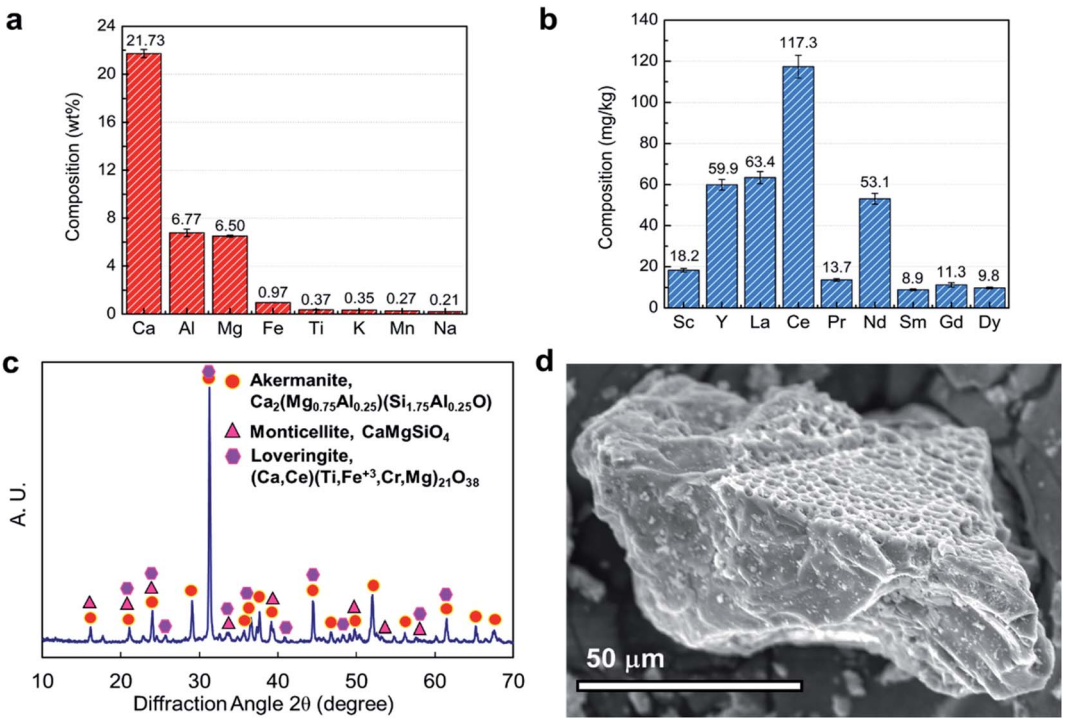

Fig. 1 Compositional, mineralogical, and morphological characteristics of the BF slag. (a) Bulk elemental composition obtained by *aqua regia* digestion followed by ICP-OES. (b) The REE elemental composition obtained by *aqua regia* digestion followed by ICP-MS. (c) X-ray diffractogram. (d) Secondary electron micrograph.

shown in Fig. 1a and b). According to the REE prices released by the United States Geological Survey,[4] scandium accounts for more than 95% of the overall value of REEs in this feed and the next critical element is neodymium. Therefore, the current study puts emphasis on the recovery of these two elements.

The crystal structure of BF slag was characterized by XRD and three major phases were detected, *i.e.*, akermanite ($Ca_2(Mg_{0.75}Al_{0.25})(Si_{1.75}Al_{0.25}O_7)$), monticellite ($CaMgSiO_4$), and loveringite ((Ca, Ce)(Ti, Fe^{3+}, Cr, Mg)$_{21}O_{38}$) (Fig. 1c). These results are consistent with the ICP-OES and XRF results, as calcium, aluminum, magnesium, and silicon are the major constituents of this BF slag. The surface morphology of BF slag particles was characterized by SEM. As shown in Fig. 1d, the surface of the BF particles is rough and porous; thus, a large surface area is available for the digestion reaction.

Acid baking–water leaching results

To assess the effect of baking temperature (X_1), acid to slag mass ratio (X_2), baking time (X_3), water to acid-baked slag ratio (X_4), agitation rate (X_5), and water to slag mass ratio (before baking) (X_6), a series of trials (19 experiments) were conducted. A summary of operating conditions and the corresponding extraction of scandium and neodymium are presented in Table 2 and the ANOVA results are provided in Table S3 in the ESI.† In these trials, the maximum extraction efficiency of scandium and neodymium was 89.4% and 78.6%, respectively.

Empirical extraction models were built by multiple Linear Least Squares Regression (mLLSR) shown in eqn (2). Fig. 2a presents the ordered factor effect coefficients for empirical extraction models for each element. Only the factors with enough significance ($\alpha = 0.05$) are provided. As shown, scandium extraction was positively affected by X_2 (acid to slag mass ratio). To explain this behavior, HSC Chemistry software (version 6.00) was used to build the Eh–pH diagram for the Sc–S–H_2O system at 25 °C. As shown in Fig. 2c, scandium is only soluble under acidic conditions, first as $Sc(SO_4)_{(aq)}^{+}$ between pH 4 and 7, and then as $Sc(SO_4)_{(aq)}^{+}$, $(ScOH)_{2(aq)}^{4+}$ and $Sc_{(aq)}^{3+}$ below pH 4; thus, increasing the acid amount or decreasing pH increases scandium solubility; hence, its extraction efficiency. Scandium extraction was negatively affected by X_1 (baking temperature) which can be explained by the fact that above 300 °C, H_2SO_4 first vaporizes and then decomposes to $SO_{3(g)}$, $SO_{2(g)}$, $H_2O_{(g)}$, and $O_{2(g)}$ (reactions (3)–(5)). This behavior is presented in the speciation diagram of H_2SO_4 as a function of temperature up to 600 °C which was obtained using FactSage software (version 7.3) (Fig. 2e).

$$H_2SO_{4(l)} = H_2SO_{4(g)} \quad (3)$$

$$H_2SO_{4(l)} = H_2O_{(g)} + SO_{3(g)} \quad (4)$$

$$H_2SO_{4(l)} = H_2O_{(g)} + SO_{2(g)} + 1/2O_{2(g)} \quad (5)$$

It should be noted that runs #4 and #6 in Table 2 had the same X_1 and X_2; thus, it was expected that they show similar extraction efficiency for scandium since X_1 and X_2 are the only primary factors affecting scandium extraction. However, it was observed that run #4 had slightly higher scandium extraction

Table 2 Overview of the experimental runs with corresponding operating parameters and extraction efficiencies for scandium and neodymium

Run #	Run description	Baking temperature X_1 (°C)	Acid to slag mass ratio X_2 (g g_{DBFS}^{-1})	Baking time X_3 (min)	Water to acid-baked slag ratio X_4 (mL g_{ABBFS}^{-1})	Agitation rate X_5 (rpm)	Water to slag mass ratio X_6 (g g_{DBFS}^{-1})	Extraction efficiency (%)	
								Sc	Nd
1		200	0.50	30	4	200	0	0.7	3.6
2		200	2.00	30	4	600	2	77.4	46.4
3		200	0.50	90	4	600	2	0.3	0.9
4	Maximum Sc extraction	200	2.00	90	4	200	0	89.4	42.4
5		200	0.50	30	16	200	2	0.7	0.6
6	Maximum Nd extraction	200	2.00	30	16	600	0	81.8	78.6
7		200	0.50	90	16	600	0	0.4	8.6
8		200	2.00	90	16	200	2	57.5	33.3
9		400	0.50	30	4	600	0	0.1	3.2
10		400	2.00	30	4	200	2	46.8	16.6
11		400	0.50	90	4	200	2	0.0	5.4
12		400	2.00	90	4	600	0	50.7	27.7
13		400	0.50	30	16	600	2	0.1	0.3
14		400	2.00	30	16	200	0	63.8	48.6
15		400	0.50	90	16	200	0	0.1	10.4
16		400	2.00	90	16	600	2	48.5	24.5
17	Center-point runs	300	1.25	60	10	400	1	58.1	51.6
18		300	1.25	60	10	400	1	60.5	54.0
19		300	1.25	60	10	400	1	54.1	49.6

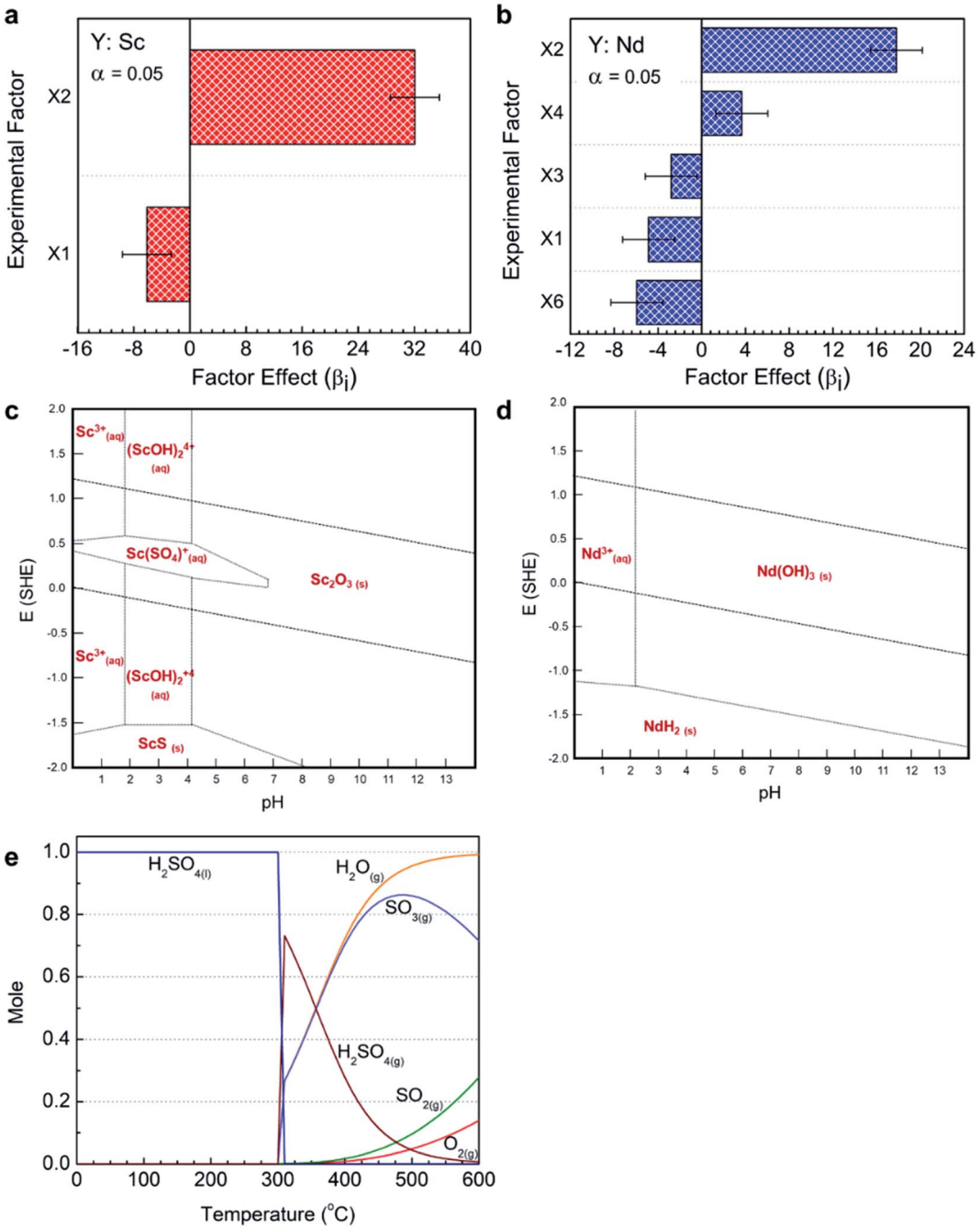

Fig. 2 Ordered charts of factor effect coefficients for the empirical extraction models for (a) scandium and (b) neodymium. Eh–pH diagram using HSC Chemistry 6.00 software for (c) scandium (Sc molality: 0.00003 mol kg^{-1}, S molality: 0.1 mol kg^{-1}) and (d) neodymium (Nd molality: 0.00002 mol kg^{-1}, S molality: 0.1 mol kg^{-1}). (e) The H_2SO_4 speciation diagram as a function of temperature using FactSage software (version 7.3).

efficiency (89.4%) compared with run #6 (81.8%). This observation can be explained by the second-order interactions of two primary factors which can further affect the extraction efficiency. In this work, these interaction terms were not considered for empirical model building because they were confounded with each other, *i.e.*, the effect of one interaction term could not be independently estimated. However, the internal analysis results showed that there exists an additional second-order interaction, $X_{12} + X_{35}$ (baking temperature × acid ratio + baking time × agitation rate) with factor effect coefficient of −5.9 for scandium extraction efficiency. This interaction was at a low (−1) factor level for run #4 while it was at a high (+1) factor level for run #6, which explains slightly higher scandium extraction in run #4 compared with run #6, considering the two runs had different baking time (X_3), water to acid-baked slag ratio (X_4), and agitation rate (X_5).

The factor effect analysis for neodymium showed that its extraction is positively affected by X_2 (acid to slag mass ratio)

and X_4 (water to acid-baked slag ratio); whereas, it is negatively affected by X_1 (baking temperature), X_3 (baking time) and X_6 (water to slag mass ratio) (Fig. 2b). To explain the positive effect of X_2, HSC Chemistry software was used to build the Eh–pH diagram of Nd–S–H_2O system at 25 °C. As shown in Fig. 2d, neodymium becomes soluble at pH below 2 as $Nd_{(aq)}^{3+}$. The positive effect of X_4 can be explained by the fact that as water amount increases, more baked slag can dissolve, leading to higher extraction efficiency. The negative effect of X_1 is due to the vaporization and decomposition of H_2SO_4, as was explained above. The negative effect of X_3 can also be explained by the same phenomenon as at high level of X_3, more time is given to H_2SO_4 to vaporize and decompose. The negative effect of X_6 is due to the fact that adding water to the slag–H_2SO_4 mixture decreases the concentration and boiling point of acid. Both of these factors have a negative effect on the sulfation reaction. By increasing X_6 from −1 (low) to +1 (high) level at the fixed high level of acid ratio (X_2), the concentration of acid decreases from 98 wt% to 49 wt% and the boiling point decreases from 337 °C to 195 °C.[34] Therefore, even if the baking temperature is at −1 (low) level (200 °C), sulfuric acid evaporates before reaching the set temperature and reacting with the slag particles at high level of X_6.

Optimization and validation of ABWL process

On the basis of the factor effect coefficients presented in Fig. 2a, b and ESI Table S4,† an empirical extraction model was built for each element using eqn (1) and (2) to predict the extraction efficiency under certain conditions. Two validation tests were carried out to assess the applicability of the models. The experimental conditions and results are provided in ESI Tables S5 and S6,† respectively. The results of the two validation tests were in good agreement with the model predicted values, having the absolute average relative deviation (AARD) of 9.8% and 11.4%, respectively. This indicates that these empirical models are suitable to be used for process optimization. The acid baking–water leaching process was then optimized with the objective of maximizing scandium and neodymium extraction. The conditions that satisfy this scenario were baking temperature of 200 °C, acid to slag mass ratio of 2 g g_{DBFS}^{-1}, baking time of 30 min, water to acid-baked slag ratio of 16 mL g_{ABBFS}^{-1}, agitation rate of 200 rpm, and water to slag mass ratio of 0 g g_{DBFS}^{-1}. Under these conditions, 82.5% scandium extraction and 80.6% neodymium extraction were achieved. The results indicate that the empirical model can successfully predict the optimum operating conditions of the process and the corresponding extraction efficiencies. In this process, some bulk metals such as aluminum, magnesium, iron, and manganese were co-

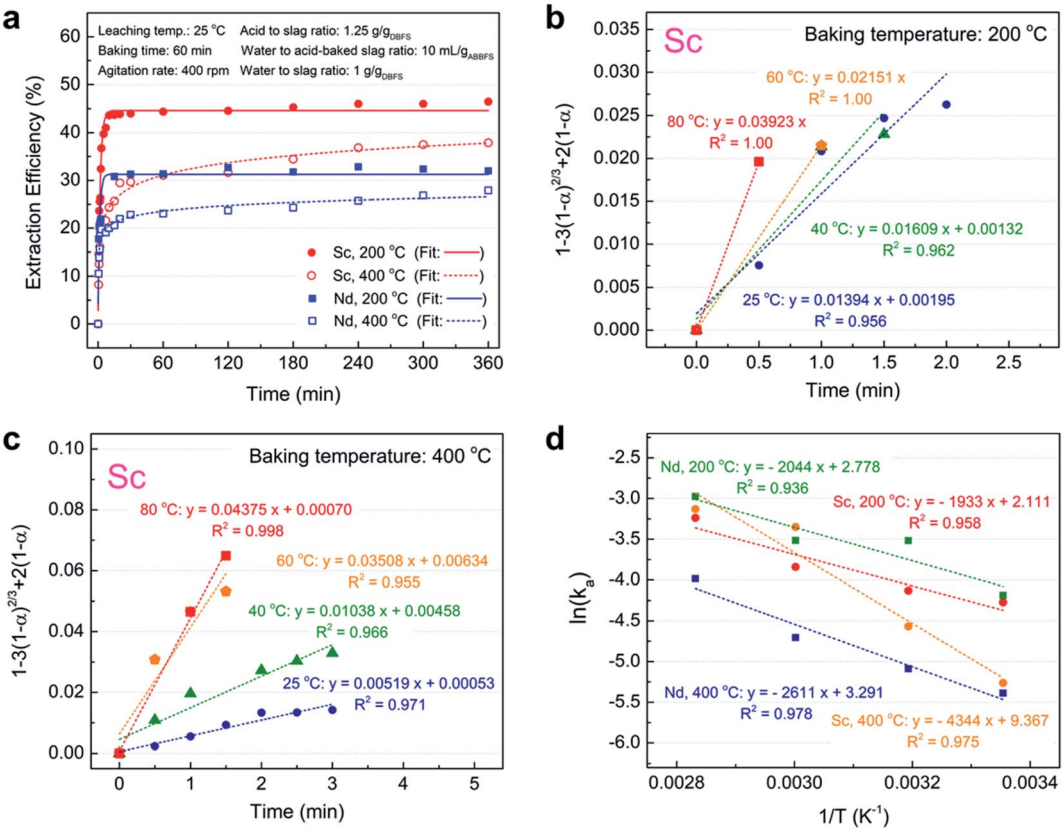

Fig. 3 (a) Extraction efficiency of scandium and neodymium during water leaching at 25 °C as a function of time for samples baked at 200 °C and 400 °C. (b) Plots of $[1 - 3(1 - \alpha)^{2/3} + 2(1 - \alpha)]$ *versus* time at various leaching temperatures for scandium for the sample baked at 200 °C. (c) Plots of $[1 - 3(1 - \alpha)^{2/3} + 2(1 - \alpha)]$ *versus* time at different leaching temperatures for scandium for the sample baked at 400 °C. (d) Arrhenius equation plots to determine the apparent activation energy (E_a) of the water leaching reactions of scandium and neodymium for samples baked at 200 °C and 400 °C.

extracted into the final leachate; thus, future work would focus on selective separation of scandium and neodymium.

Kinetic investigation of water leaching

To investigate the effect of baking temperature on the kinetics of water leaching process, two kinetic experiments were conducted on samples baked at 200 °C and 400 °C under ambient conditions, while other factors were kept at zero (mid) level (acid to slag ratio of 1.25 g g_{DBFS}^{-1}, baking time of 60 min, water to acid-baked slag ratio of 10 mL g_{ABBFS}^{-1}, agitation rate of 400 rpm, and water to slag ratio (before baking) of 1 g g_{DBFS}^{-1}). As shown in Fig. 3a, the kinetics of water leaching for the sample baked at 200 °C is very fast and 10 min is enough to reach equilibrium. On the contrary, the kinetics of water leaching for the sample baked at 400 °C was slower, taking more than 4 h to reach equilibrium.

To elucidate the mechanism of scandium and neodymium leaching process in water from acid-baked BF slag, the initial stage of water leaching at four temperatures between 25 and 80 °C was modeled using the shrinking core model.[35] Eqn (6)–(8) present the most common forms of this model and eqn (9) is the Arrhenius equation which is used to determine the apparent activation energy of the reaction.

$$\alpha = k_a t \quad (6)$$

$$1 - 3(1-\alpha)^{2/3} + 2(1-\alpha) = k_a t \quad (7)$$

$$1 - (1-\alpha)^{1/3} = k_a t \quad (8)$$

$$k_a = A \exp\left(-\frac{E_a}{RT}\right) \quad (9)$$

where α is the extraction efficiency at time t (min), k_a is the apparent rate constant (min^{-1}), A is the frequency factor, E_a is the apparent activation energy (J mol^{-1}), R is the universal gas constant (8.314 J mol^{-1} K^{-1}), and T is the absolute temperature (K). Eqn (6) describes the leaching process of solid particles with spherical geometry when the rate determining step is the diffusion of water through the boundary layer, while eqn (7) describes the case in which diffusion of water through the firm solid product (so-called the ash layer) is the rate determining step and eqn (8) describes the case in which chemical reaction at the particle surface is the rate determining step.

The extraction efficiencies of scandium and neodymium were fitted to eqn (6)–(8) and the coefficients of determination (R^2) were compared. The results indicated that eqn (7) has the highest R^2 value regardless of the baking temperature, suggesting that the rate determining step of the water leaching kinetics is the diffusion of water through the ash layer (Fig. 3b and c).

Plotting ln k_a as a function of $1/T$ for samples baked at 200 °C and 400 °C resulted in straight lines with R^2 above 0.936, as shown in Fig. 3d. On the basis of the slope of the lines, the apparent activation energy of scandium and neodymium leaching process was determined to be 16.1 and 17.0 kJ mol^{-1} for the sample baked at 200 °C and 36.1 and 21.7 kJ mol^{-1} for the sample baked at 400 °C. These results are in line with the results of previous studies showing an ash diffusion-controlled reaction for REE leaching from phosphogypsum[21] and bauxite residue.[16,25] The lower apparent activation energies at 200 °C compared with those at 400 °C are in agreement with faster kinetic results for the 200 °C-baked sample.

Mechanistic investigation of the digestion process during acid baking process

In BF slag, scandium and neodymium are present in trace amounts; thus, elucidation of their digestion mechanism requires observation of mineralogical and morphological changes of major element-bearing phases during digestion in acid baking process. To this end, the pairwise correlations between extraction efficiency of scandium and neodymium and that of bulk metals (Al, Mg, Ti, Fe, Ca, and Mn) were assessed (ESI Table S7†) and the results indicated that the extraction efficiency of scandium and neodymium is highly correlated with that of aluminum ($R^2 = 0.95$ and 0.85, respectively), suggesting that they likely exist in the aluminum-bearing phases.

To investigate the mineralogical changes of the BF slag during acid baking and water leaching, XRD was utilized and the results indicated that akermanite ($Ca_2(Mg_{0.75}Al_{0.25})(Si_{1.75}Al_{0.25}O_7)$) which is the major phase of aluminum in the feed is digested and replaced with sulfate phases (Fig. 4a). Baking at 200 °C with an acid to slag ratio of 2.00 g g_{DBFS}^{-1} results in the formation of alunogen ($(Al(H_2O)_6)_2(SO_4)_3(H_2O)_{4.4}$), pickeringite ($MgAl_2(SO_4)_4 \cdot 22H_2O$), and anhydrite ($CaSO_4$). Although not presented, an amorphous magnesium sulfate hydrate ($MgSO_4 \cdot xH_2O$) was possibly formed as well considering the presence of anhydrous $MgSO_4$ in the sample baked at 400 °C. The overall chemical reaction is presented in reaction (10).

$$\begin{aligned} Ca_2(Mg_{0.75}Al_{0.25})(Si_{1.75}Al_{0.25}O_7)_{(s)} + 3.5H_2SO_{4(l)} \\ = (y-0.5)(Al(H_2O)_6)_2(SO_4)_3(H_2O)_{4.4(s)} \\ + (0.75-y)MgAl_2(SO_4)_4 \cdot 22H_2O_{(s)} + 2CaSO_{4(s)} \\ + yMgSO_4 \cdot xH_2O_{(s)} + 1.75SiO_{2(l)} \\ + (5.6y - xy - 4.8)H_2O_{(g)} \ (T = 200\ ^\circ C) \end{aligned} \quad (10)$$

At higher baking temperature of 400 °C, $(Al(H_2O)_6)_2(SO_4)_3(H_2O)_{4.4}$ transforms into anhydrous $Al_2(SO_4)_3$, following reaction (11). Because scandium and neodymium are associated with aluminum and akermanite ($Ca_2(Mg_{0.75}Al_{0.25})(Si_{1.75}Al_{0.25}O_7)$) is the major aluminum phase in the feed, the phase transformation from akermanite to alunogen ($(Al(H_2O)_6)_2(SO_4)_3(H_2O)_{4.4}$) (reaction (10)) and to $Al_2(SO_4)_3$ could explain the digestion mechanism.

$$\begin{aligned} (Al(H_2O)_6)_2(SO_4)_3(H_2O)_{4.4} \\ = Al_2(SO_4)_3 + 16.4H_2O \ (T > 250\ ^\circ C) \end{aligned} \quad (11)$$

One thing to note about $(Al(H_2O)_6)_2(SO_4)_3(H_2O)_{4.4}$ is that the number of water molecules in this structure is known to vary from 16 to 18 because water molecules are loosely bound and can be readily released with a slight change in humidity or temperature.[36] The crystal structure of $(Al(H_2O)_6)_2(SO_4)_3(H_2O)_{4.4}$ is presented in Fig. 4b. As shown, $(Al(H_2O)_6)_2(SO_4)_3(H_2O)_{4.4}$ has

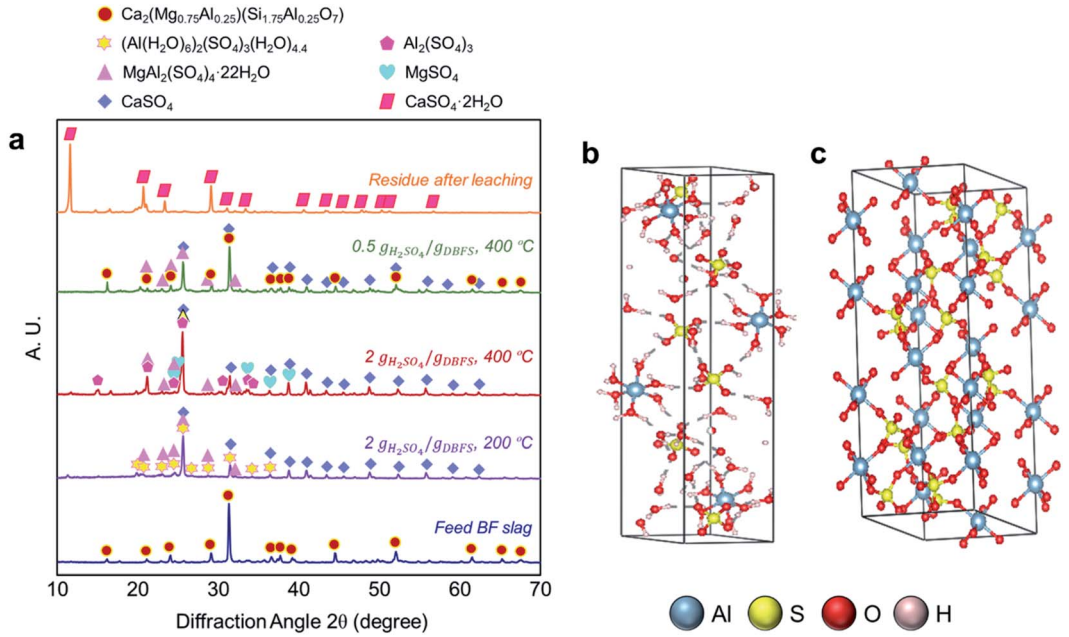

Fig. 4 (a) X-ray diffractogram of the BF slag feed, acid-baked BF slag samples, and residue after water leaching. (b) Schematic representation of crystal structure of $(Al(H_2O)_6)_2(SO_4)_3(H_2O)_{4.4}$ using VESTA software. (c) Schematic representation of crystal structure of $Al_2(SO_4)_3$ using VESTA software.

a triclinic structure in which aluminum atoms are surrounded by six water molecules forming $Al(H_2O)_6$ octahedra. These octahedra are interconnected with the sulfate tetrahedra through weak hydrogen bonds which can easily break.[37,38] The formation of $(Al(H_2O)_6)_2(SO_4)_3(H_2O)_{4.4}$ and its decomposition by humidity can explain the rapid water leaching kinetics for the sample baked at 200 °C.

At higher baking temperature of 400 °C, $(Al(H_2O)_6)_2(SO_4)_3(H_2O)_{4.4}$ transforms to $Al_2(SO_4)_3$ according to reaction (11), releasing water vapor. Anhydrous $Al_2(SO_4)_3$ has a hexagonal structure with strong ionic bonds and no hydrogen bonding (Fig. 4c); hence, water cannot readily infiltrate in this structure; thus, the kinetics of water leaching for the sample baked at 400 °C is slower.

To investigate the effect of acid to slag ratio on the mineralogical change, a sample that was baked at 400 °C with acid to slag ratio of 0.50 g g_{DBFS}^{-1} was also characterized by XRD. As shown in Fig. 4a, at lower acid to slag ratio, the sample contained unreacted $Ca_2(Mg_{0.75}Al_{0.25})(Si_{1.75}Al_{0.25}O_7)$ along with $MgAl_2(SO_4)_4{\cdot}22H_2O$ and $CaSO_4$. This indicates that the acid amount is an important controlling factor in the digestion process and if the acid amount is not enough, the reaction will not take place. This is in agreement with the observed positive effect of acid to slag mass ratio on the extraction of scandium and neodymium (Fig. 2a and b).

The microfluidic transport environment in silicate-rich feeds can result in silica gel polymerization, which negatively affects the leaching process. As shown in Fig. 4a, no silicon bearing phase was detected in the acid-baked sample; hence, no silica gel formation was observed during the water leaching step, which is consistent with our previous study on the steelmaking slag valorization process.[39] The residue after the water leaching step was mainly composed of gypsum ($CaSO_4{\cdot}2H_2O$), which can be utilized in manufacture of wallboard, cement, plaster of Paris, soil conditioning, and a hardening retarder in portland cement.

To identify the thermal events and related chemical reactions during the acid baking process, a sample containing BF slag, sulfuric acid, and water with an acid ratio of 1.25 g g_{DBFS}^{-1} (mid level) and water ratio of 1.00 g g_{DBFS}^{-1} (mid level) was characterized using thermogravimetric analysis. The TG-DSC

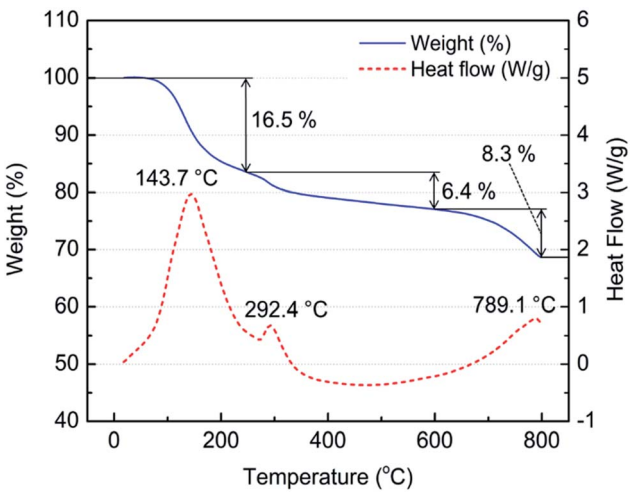

Fig. 5 The TG-DSC results of a sample containing BF slag, sulfuric acid, and water with an acid ratio of 1.25 g g_{DBFS}^{-1} and water ratio of 1.00 g g_{DBFS}^{-1} under 80% N_2 and 20% O_2 atmosphere. The heating rate was set at 20 °C min^{-1}.

results showed three main endothermic events in the temperature range of 20 to 800 °C (Fig. 5). The first event occurred between 100 and 250 °C with an endothermic peak at 143.7 °C and a weight loss of 16.5%. This change is attributed to water and sulfuric acid evaporation along with sulfation reactions forming $(Al(H_2O)_6)_2(SO_4)_3(H_2O)_{4.4}$, $MgSO_4 \cdot xH_2O$, $MgAl_2(SO_4)_4 \cdot 22H_2O$, and $CaSO_4$ (Fig. 4a). The second event with corresponding weight loss of 6.4% is attributed to the dehydration of $(Al(H_2O)_6)_2(SO_4)_3(H_2O)_{4.4}$ at 250 °C, $MgSO_4 \cdot xH_2O$ at 330–400 °C, and $MgAl_2(SO_4)_4 \cdot 22H_2O$ at around 400 °C as presented in Fig. 4a.[36,40,41] The offset temperatures for the decomposition of $Al_2(SO_4)_3$ and dehydrated $MgAl_2(SO_4)_4 \cdot 22H_2O$ are 750 °C and 700 °C, respectively, and these decomposition reactions contribute to the final endothermic event at 781 °C with the associated weight loss of 8.3%.

Conclusions

In this study, an acid baking–water leaching process was developed to recover scandium and neodymium from blast furnace ironmaking slag. A systematic investigation was performed to study the effect of six operating parameters, namely baking temperature, acid to slag mass ratio, baking time, water to acid-baked slag ratio, agitation rate, and water to slag mass ratio (before baking) on extraction. It was shown that acid to slag mass ratio has the highest positive effect on extraction because in sulfate media, scandium is only soluble under acidic conditions and neodymium becomes soluble at pH below 2; thus, increasing acid ratio decreases pH of the leachate; hence, increasing the solubility of scandium and neodymium, and in turn, the extraction efficiency. Baking temperature showed a negative impact on extraction because sulfuric acid evaporates at 300 °C and then decomposes to $SO_{3(g)}$, $SO_{2(g)}$, $H_2O_{(g)}$, and $O_{2(g)}$. The pairwise correlations between extraction efficiency of scandium and neodymium and that of bulk metals indicated that the extraction efficiency of scandium and neodymium is highly correlated with that of aluminum; hence, it is expected that they are associated with aluminum-bearing phases in the feed.

The mechanism of the digestion process was elucidated by baking the feed at 200 and 400 °C. It was shown that at low baking temperature, akermanite ($Ca_2(Mg_{0.75}Al_{0.25})(Si_{1.75}Al_{0.25}O_7)$) that is the major aluminum phase in the feed transforms into alunogen ($(Al(H_2O)_6)_2(SO_4)_3(H_2O)_{4.4}$) that is held together with weak hydrogen bonds. Water can easily infiltrate in this structure; hence the kinetics of water leaching for this sample is very fast (<10 min). On the contrary, at 400 °C alunogen ($(Al(H_2O)_6)_2(SO_4)_3(H_2O)_{4.4}$) transformed into $Al_2(SO_4)_3$ with strong ionic bonds; thus, the kinetics of water leaching for this samples was slow (>4 h). Kinetic analysis of the water leaching step sheds light on the process mechanism, and it was shown that the diffusion of water into the ash layer is the rate determining step. The results of this study show the feasibility of recovering scandium and neodymium from stockpiled BF slag with less acidic waste generation compared with the direct leaching process. Despite being energy intensive, acid baking–water leaching is an efficient process for scandium and neodymium recovery, leading to 82.5% and 80.6% extraction, respectively with fast kinetics under optimum operating conditions.

Author contributions

G. A. conceived and supervised the research. J. K. designed and performed the experiments and analyzed the results. Both authors contributed to writing and revising the manuscript and have given approval to the final version of the manuscript.

Conflicts of interest

There are no conflicts to declare.

Acknowledgements

This work was supported by Natural Sciences and Engineering Research Council of Canada (NSERC) [grant number 503603]; Ontario Centres of Excellence (OCE) [grant number 503616]; and Tenova Goodfellow [grant number 503604]. We thank Mr Vittorio Scipolo from Tenova Goodfellow for the collaboration throughout the project. We thank Mr Kok Long Ng for help with SEM-EDS and Dr Raiden Acosta for help with XRF, XRD, TG-DSC, and PSA.

References

1 E. A. Olivetti and J. M. Cullen, *Science*, 2018, **360**, 1396–1398.
2 D. Raabe, C. C. Tasan and E. A. Olivetti, *Nature*, 2019, **575**, 64–74.
3 *Steel Statistical Yearbook*, World Steel Association, Brussels, Belgium, 2020.
4 U.S. Geological Survey, *Mineral Commodity Summaries 2020*, U.S. Geological Survey, 2020.
5 K. Horii, N. Tsutsumi, Y. Kitano and T. Kato, *Processing and reusing technologies for steelmaking slag*, 2013, vol. 805.
6 H. G. van Oss, *Iron and steel slag*, 2002.
7 D. Morian, T. Van Dam and R. Perera, *Use of air-cooled blast furnace slag as coarse aggregate in concrete pavements*, 2012.
8 E. Özbay, M. Erdemir and H. I. Durmuş, *Constr. Build. Mater.*, 2016, **105**, 423–434.
9 J. Du, Y. Bu, S. Guo, L. Tian and Z. Shen, *RSC Adv.*, 2017, **7**, 36460–36472.
10 S. He, H. Sun, D. g Tan and T. Peng, *Procedia Environ. Sci.*, 2016, **31**, 977–984.
11 M. Kasina and M. Michalik, *Mineralogia*, 2017, **28**, 15–25.
12 D. M. Proctor, K. A. Fehling, E. C. Shay, J. L. Wittenborn, J. J. Green, C. Avent, R. D. Bigham, M. Connolly, B. Lee, T. O. Shepker and M. A. Zak, *Environ. Sci. Technol.*, 2000, **34**, 1576–1582.
13 H. Jiang, H. Guo, P. Li, Y. Li and B. Yan, *RSC Adv.*, 2019, **9**, 6054–6063.
14 K. Binnemans, Y. Pontikes, P. T. Jones, T. Van Gerven and B. Blanpain, in *Slag valorisation symposium: the transition to sustainable materials management*, 2013, pp. 191–205.

15 Abhilash, P. Meshram, S. Sarkar and T. Venugopalan, *Miner. Metall. Process.*, 2017, **34**, 178–182.
16 S. Reid, J. Tam, M. Yang and G. Azimi, *Sci. Rep.*, 2017, **7**, 1–9.
17 R. G. Eggert, *Nat. Chem.*, 2011, **3**, 688–691.
18 T. Vander Hoogerstraete, B. Blanpain, T. Van Gerven and K. Binnemans, *RSC Adv.*, 2014, **4**, 64099–64111.
19 X. Du and T. E. Graedel, *Sci. Rep.*, 2011, **1**, 1–4.
20 K. Binnemans, P. Tom, B. Blanpain, T. Van Gerven and Y. Pontikes, *J. Cleaner Prod.*, 2015, **99**, 17–38.
21 M. Walawalkar, C. K. Nichol and G. Azimi, *Hydrometallurgy*, 2016, **166**, 195–204.
22 C. R. Borra, B. Blanpain, Y. Pontikes, K. Binnemans and T. Van Gerven, *J. Sustain. Metall.*, 2016, **2**, 365–386.
23 R. Q. Honaker, W. Zhang and J. Werner, *Energy Fuels*, 2019, **33**, 5971–5980.
24 M. Peiravi, L. Ackah, R. Guru, M. Mohanty, J. Liu, B. Xu, X. Zhu and L. Chen, *Miner. Metall. Process.*, 2017, **34**, 170–177.
25 J. Anawati and G. Azimi, *Waste Manag.*, 2019, **95**, 549–559.
26 J. He, Y. Li, X. Xue, H. Ru, X. Huang and H. Yang, *RSC Adv.*, 2017, **7**, 14053–14059.
27 G. Alkan, B. Yagmurlu, S. Cakmakoglu, T. Hertel, Ş. Kaya, L. Gronen, S. Stopic and B. Friedrich, *Sci. Rep.*, 2018, **8**, 1–11.
28 A. Lambert, J. Anawati, M. Walawalkar, J. Tam and G. Azimi, *ACS Sustain. Chem. Eng.*, 2018, **6**, 16471–16481.
29 R. M. Rivera, B. Ulenaers, G. Ounoughene, K. Binnemans and T. Van Gerven, *Miner. Eng.*, 2018, **119**, 82–92.
30 C. R. Borra, J. Mermans, B. Blanpain, Y. Pontikes, K. Binnemans and T. Van Gerven, *Miner. Eng.*, 2016, **92**, 151–159.
31 F. Soltani, M. Abdollahy, J. Petersen, R. Ram, M. Becker, S. M. Javad Koleini and D. Moradkhani, *Hydrometallurgy*, 2018, **177**, 66–78.
32 J. Demol, E. Ho and G. Senanayake, *Hydrometallurgy*, 2018, **179**, 254–267.
33 P. Meshram, H. Somani, B. D. Pandey, T. R. Mankhand, H. Deveci and Abhilash, *J. Cleaner Prod.*, 2017, **157**, 322–332.
34 Sciencelab.com, *Material safety data sheet sulfuric acid 50% (w/w) solution MSDS*, 2016.
35 O. Levenspiel, *Chemical Reaction Engineering*, John Wiley & Sons, 3rd edn, 1999.
36 V. Kahlenberg, D. E. Braun, H. Krüger, D. Schmidmair and M. Orlova, *Phys. Chem. Miner.*, 2017, **44**, 95–107.
37 S. Menchetti and C. Sabelli, *Tschermaks Mineral. Petrogr. Mitt.*, 1974, **21**, 164–178.
38 J. H. Fang and P. D. Robinson, *Am. Mineral.*, 1976, **61**, 311–317.
39 J. Kim and G. Azimi, *Hydrometallurgy*, 2020, **191**, 1–10.
40 M. N. Scheidema and P. Taskinen, *Ind. Eng. Chem. Res.*, 2011, **50**, 9550–9556.
41 Z. e. Nakagawa, K. Hamano, M. Sakaguchi and S. Kanzaki, *J. Ceram. Assoc. Jpn.*, 1983, **91**, 297–303.